

1 Human pathogenic RNA viruses establish non-competing 2 lineages by occupying independent niches

3 Pascal Mutz¹⁺, Nash D. Rochman^{1+*}, Yuri I. Wolf¹, Guilhem Faure², Feng Zhang^{2,3,4,5,6}, and Eugene V.
4 Koonin^{1*}

5 ¹National Center for Biotechnology Information, National Library of Medicine, Bethesda, MD 20894

6 ²Broad Institute of MIT and Harvard, Cambridge, MA 02142; ³Howard Hughes Medical Institute,

7 Massachusetts Institute of Technology, Cambridge, MA 02139; ⁴McGovern Institute for Brain Research,

8 Massachusetts Institute of Technology, Cambridge, MA 02139; ⁵Department of Brain and Cognitive

9 Sciences, Massachusetts Institute of Technology, Cambridge, MA 02139; and ⁶Department of Biological

10 Engineering, Massachusetts Institute of Technology, Cambridge, MA 02139

11

12

13 ⁺Authors contributed equally

14 *For correspondence: nash.rochman@nih.gov, zhang@broadinstitute.org, koonin@ncbi.nlm.nih.gov

15

16 Keywords: effective population size, human RNA viruses, pandemic, globalization,

17 Influenza, SARS-CoV-2, viral phylodynamics

18

19

20 **Abstract**

21

22 Many pathogenic viruses are endemic among human populations and can cause a
23 broad variety of diseases, some potentially leading to devastating pandemics. How virus
24 populations maintain diversity and what selective pressures drive population turnover, is
25 not thoroughly understood. We conducted a large-scale phylodynamic analysis of 27
26 human pathogenic RNA viruses spanning diverse life history traits in search of unifying
27 trends that shape virus evolution. For most virus species, we identify multiple, co-
28 circulating lineages with low turnover rates. These lineages appear to be largely
29 noncompeting and likely occupy semi-independent epidemiological niches that are not
30 regionally or seasonally defined. Typically, intra-lineage mutational signatures are
31 similar to inter-lineage signatures. The principal exception are members of the family
32 *Picornaviridae*, for which mutations in capsid protein genes are primarily lineage-
33 defining. The persistence of virus lineages appears to stem from limited outbreaks
34 within small communities so that only a minor fraction of the global susceptible
35 population is infected at any time. As disparate communities become increasingly
36 connected through globalization, interaction and competition between lineages might
37 increase as well, which could result in changing selective pressures and increased
38 diversification and/or pathogenicity. Thus, in addition to zoonotic events, ongoing
39 surveillance of familiar, endemic viruses appears to merit global attention with respect to
40 the prevention or mitigation of future pandemics.

41

42 **Significance**

43 Numerous pathogenic viruses are endemic in humans and cause a broad variety of
44 diseases, but what is their potential of causing new pandemics? We show that most
45 human pathogenic RNA viruses form multiple, co-circulating lineages with low turnover
46 rates. These lineages appear to be largely noncompeting and occupy distinct
47 epidemiological niches that are not regionally or seasonally defined, and their
48 persistence appears to stem from limited outbreaks in small communities so that a
49 minor fraction of the global susceptible population is infected at any time. However, due
50 to globalization, interaction and competition between lineages might increase,

51 potentially leading to increased diversification and pathogenicity. Thus, endemic viruses
52 appear to merit global attention with respect to the prevention of future pandemics.

53

54

55

56 **Introduction**

57 Viruses, ubiquitous across the tree of life, occupy an astounding diversity of ecological
58 niches (1-3). Viral niches are primarily defined by the behavior and immunity of the
59 respective hosts and are often the subject of deep, but narrow investigation (4, 5). In
60 this work, we sought to uncover common trends at relatively short evolutionary
61 distances by studying the microevolution of human pathogenic RNA viruses. The
62 devastating COVID-19 pandemic has made it abundantly clear that understanding these
63 microevolutionary features is of vital importance not only to forward our understanding
64 of virology in general but to inform appropriate public health measures during a
65 pandemic (6, 7).

66 Viral populations explore their viable sequence space defined both by intrinsic
67 constraints and those imposed by host behavior (8) through the accumulation of
68 mutations, potentially leading to diversification (9). A single host species can offer
69 multiple independent niches that are explored by distinct virus subpopulations. Niches
70 can be formed and maintained through regional or seasonal separation. Regional
71 separation of subpopulations has been demonstrated, for example, for yellow fever
72 virus (YFV) (10, 11). At sufficiently long evolutionary distances, niches can be defined
73 by immunological differences, which enable a viral subpopulation to overcome immune
74 cross-protection, allowing the same host to be infected by multiple subpopulations
75 largely independent of prior infections. This phenomenon has been demonstrated for
76 enteroviruses with many co-circulating serotypes (12). These immunological niches do
77 not need to be spatially or temporally segregated.

78 Generally, niches are not necessarily static entities and can overlap or merge
79 depending on dissemination rates, transmission modes, and other life history traits (2).
80 When outbreaks are limited to small communities so that only a small fraction of the
81 global susceptible population is infected at any time, niches can form that are not
82 regionally or seasonally defined but are still maintained through a combination of spatial
83 and temporal separation at a local scale. Thus, the maintenance of these viral niches is
84 highly sensitive to changes in host behavior. The number and sequence diversity of
85 such lineages depends on constraints intrinsic to viral biology as well as host
86 behavior (13, 14). For example, there is a sharp contrast between the emergence of

87 immunological niches among measles morbilli virus (MMV) and influenza A virus (IAV)
88 strain H3N2 (named H3N2 here). Through rapid antigenic drift and shift that involve a
89 non-human host reservoir, IAV is able to overcome adaptive-immune protection, despite
90 infecting a substantial fraction of the susceptible host population each year (15). As a
91 consequence, H3N2 goes through phases of stasis, in which neutral evolution and
92 purifying selection are dominant; parallel lineages are established; and population
93 diversity grows. Once the pool of naïve hosts shrinks, the competition between lineages
94 intensifies, resulting in a short phase of strong positive selection that favors one lineage
95 to replace all others (16-18). In contrast, no such antigenic drift has been observed for
96 MMV, and parallel MMV lineages do not replace each other, but rather stably co-exist
97 (17, 19).

98 The persistence of multiple, co-existing viral lineages implies minimal inter-
99 lineage competition. When such lineages are maintained through spatial or temporal
100 separation, increased host-host or host-vector contact can result in the merger between
101 and competition among multiple lineages. Climate change can support the spread and
102 mixing of previously separated vectors, which could carry distinct viral lineages. With
103 more vectors, the dissemination rate can rise, decreasing the number of susceptible
104 hosts, and increasing competition globally (2). This can result in accelerated lineage
105 turnover of human and agricultural pathogens, with the potential for substantial
106 epidemiological and economic impact (20).

107 We sought to identify unifying trends of lineage emergence, persistence, and
108 turnover among human pathogenic RNA viruses and to characterize the niches
109 occupied by these lineages through phylodynamic analysis (21). Taking advantage of
110 the substantial recent progress in virus genome sequencing (22), we constructed
111 phylogenetic trees for the genomes of all monopartite human pathogenic RNA viruses
112 for which extensive genome sequence information was available. These phylogenies
113 were employed to assess the selection pressures affecting the evolution of these
114 viruses through an analysis of the ratio of non-synonymous to synonymous substitution
115 rates (dN/dS), and to estimate the effective population size (Ne) and the census
116 population size (N) for each. The viruses studied here are of clear epidemiological
117 relevance, span a broad variety of life history traits (2, 23), and thus seem suitable to

118 reveal unifying trends in the microevolution of RNA viruses. Our analysis of these
119 viruses indicates that most form multiple, coexisting, non-competing lineages which
120 appear to occupy independent niches.

121

122 **Results**

123 **Data aggregation**

124 Despite the substantial progress of the past several years (22), the available numbers of
125 (nearly) complete genome sequences of human pathogenic RNA viruses differ widely
126 among viral species. In the data set for the present analysis, we included only those
127 species for which 200 or more (nearly) complete genome sequences, with at least 50
128 isolated from a human host, were available in the NCBI virus database (24) or GISAID
129 for Severe acute respiratory syndrome-related coronavirus 2 (SARS-CoV-2) (25) (Fig.
130 1). These criteria excluded viruses which are widespread, for example lyssa
131 rhabdovirus and rubella virus, but for which few (nearly) complete genomes were
132 available as well as comparatively rare, even if highly pathogenic, viruses including
133 some Ebola virus species (Zaire, but not Reston or Sudan, was included) and Marburg
134 virus.

135 Only monopartite RNA viruses were considered in order to exclude potential
136 effects of segment reassortment and enable the construction of a single, unambiguous
137 phylogeny. This restriction excluded 6 species with many genomes available: three
138 Influenza viruses (A, B, and C), Reovirus, Lassa mammarenavirus, and Dabie
139 bandavirus. We further omitted HIV given its retro-transcribing replication strategy.
140 Altogether, our dataset included 26 monopartite virus species. We added IAV H3N2 to
141 this group (with a phylogeny constructed from hemagglutinin) as a thoroughly studied
142 reference virus (14, 16, 17). The 27 viruses analyzed here cover a broad variety of viral
143 lifestyles and ecological constraints and have been subject to varied countermeasures
144 including vaccination (Supplementary Data, Table S1). This diversity enables the
145 exploration of potential unifying trends of viral lineage turnover and niche formation.

146 Sequences were aligned using MAFFT(26), and with the exception of SARS-
147 CoV-2 and H3N2, for which the large number of sequences necessitated an iterative
148 strategy, phylogenetic trees were constructed using IQ-TREE (27) (see Brief Methods

149 and Extended Methods in the SI Appendix for details). For most of viruses, the resulting
150 trees included several large, clearly distinguishable clades (Fig. 1) that in some cases
151 corresponded to known sero- or genotypes (for example, Dengue virus, DENV,
152 serotypes 1-4).

153

154 **Low rates of lineage turnover among human RNA viruses**

155 The major virus clades and the smaller lineages contained within them are
156 subject to turnover whereby an older lineage goes extinct, being gradually replaced by
157 individuals from a newer lineage. Trees with high turnover rates are often described as
158 “cactus”- or “ladder”-like, and in the limit of extreme turnover, as “caterpillar” trees,
159 whereas those with low turnover are often described as “bush”-like, with ultrametric
160 trees representing the limit of no turnover (14, 17). In an effort to explicitly measure
161 lineage turnover (without relying solely on global measures such as coalescence rate
162 (17), which is also estimated), we first sought to establish how many isolates, and
163 distributed on the tree in what way, constitute a lineage. This information is important, in
164 large part because varying substitution rates across the tree complicate the estimation
165 of global lineage turnover (9, 28). We defined lineages as monophyletic groups of
166 sequences separated by periods (branches of the tree) with apparently different
167 substitution rates and within which the sequencing date and the distance to the tree root
168 are significantly correlated (see Brief Methods and Extended Methods in the SI
169 Appendix for details). Lineages cannot be defined in this way to encompass all
170 sequences and Fig. S1 shows the fraction of sequences included in correlated lineages
171 for each virus. Arguably, significantly different substitution rates mark different selective
172 environments and may reflect movement into distinct epidemiological niches. Because
173 there are no apparent periods of different substitution rates within each lineage and,
174 consequently, high-confidence date-constrained genealogical trees with a single
175 substitution rate could be fit for each (see below), we denote these “genealogical
176 lineages” (GL).

177 Multiple GL were identified in this manner for most viruses (Figs. S2-7), as
178 illustrated in Fig. 2A,B for the three lineages of Enterovirus D (EVD). For human
179 Betacoronavirus 1 (BCoV1), Ebola Zaire (Ebola), MERS (Middle East respiratory

180 syndrome-related coronavirus), H3N2, SARS-CoV-2, and Zika virus (ZIKV), the majority
181 of the phylogeny comprised a single GL. Thus, the entire population of each of these
182 viruses might occupy a single epidemiological niche at any point in time (which may be
183 subject to rapid lineage turnover as is the case for H3N2). For Mumps rubulavirus
184 (MRV) and YFV, the GL identified were not large enough for subsequent analysis.
185 When interpreting our observation of a single GL for Ebola, it should be noted that more
186 than half of the Ebola isolates stem from the 2014-2016 outbreak in Sierra Leone,
187 Liberia, and Guinea (29), the common assumption being that each individual Ebola
188 outbreak stems from an individual zoonotic spillover event (30).

189 Having identified the virus GLs, we quantified lineage turnover using the
190 Shannon entropy of the GL distribution over time, S_t , as well as travelling up the tree
191 from root to leaf, S_d . For this analysis, only sequences included within a GL were
192 considered. First, sliding windows (indexed over j) containing the closest 5% of all
193 isolates to the specified date, w_t^j , (from the date of the earliest isolated sequence to the
194 latest) or distance to the tree root, w_d^j , were established and the GL distribution within
195 each window was obtained (Fig. 2C). Next, the probability that a sequence, x , within
196 each window belongs to the i^{th} GL was computed: $P_{t,d}^j(x \in GL_i | x \in w_{t,d}^j)$. The Shannon
197 entropy of the GL distribution was then calculated using log base N equal to the number
198 of GLs identified within the tree (and yielding a maximum value of 1):

$$199 S_{t,d}^j = - \sum_{i=1}^N P_{t,d}^j(x \in GL_i | x \in w_{t,d}^j) \log_N \left(P_{t,d}^j(x \in GL_i | x \in w_{t,d}^j) \right)$$

200 Finally, the mean over all windows was computed for each tree: $\langle S_{t,d}^j \rangle_j$ (Fig. 2D). A
201 mean entropy near 0 corresponds to a phylogeny composed of clades that rapidly
202 displace one another (although effects of sampling bias cannot be excluded). A mean
203 entropy near 1 corresponds to a phylogeny, in which all clades are uniformly distributed
204 at every time point. We observed $\langle S_t^j \rangle_j > \langle S_d^j \rangle_j$ in all but one case (HDV) indicating that
205 entropy is greater than that expected from analysis of the tree structure with no known
206 dates of isolation. This observation coupled with the generally high mean entropy
207 suggests that most of the analyzed viruses evolve with low rates of lineage turnover.

208 To further quantify lineage turnover, we constructed date-constrained
209 genealogical trees. As suggested above, GLs are separated by periods (branches of the
210 tree) with apparently different substitution rates. These branches are often deep within
211 the tree and are sparsely populated with leaves (if at all), making the assignment of a
212 global model for substitution rates statistically dubious and highlighting the importance
213 of rates inferred for individual GLs. Date constrained trees were produced using a least-
214 square distance approach based on the date of isolation for each sequence (31). A
215 mutation rate and the date of the last common ancestor (LCA) were estimated for all
216 global trees and each GL individually (Fig. 3A). Samples without a known date of
217 isolation introduce additional uncertainty into the calculation and can result in future-
218 dated portions of the genealogical tree (see Brief Methods and Extended Methods in the
219 SI Appendix for details). GLs tend to accumulate over time, with few if any extinction
220 events (Fig. 3B). Note that the apparent decline of parallel GLs for many viruses in
221 recent years (approximately 2016-present) is most likely a sampling artefact although, in
222 principle, such decline could also point to a change in GL dynamics. These trends are
223 further indicative of low lineage turnover and suggestive of minimal competition among
224 GLs. Thus, each GL is likely to occupy a distinct niche, and we sought to identify the
225 factors that shape and maintain these niches.

226

227 **Most virus lineages are not regionally or seasonally defined**

228 Perhaps the simplest explanation for the existence of distinct niches would be
229 regional separation. To assess the role played by regionality, we examined whether
230 isolates within a single GL clustered by region. The great circle map distance between
231 pairs of isolates within each GL and between pairs of GLs was computed to retrieve the
232 mean intra- and inter-GL distance, respectively (see Brief Methods and Extended
233 Methods in the SI Appendix for details). Given that GLs do not span the entire
234 phylogeny for all viruses; were defined algorithmically without the incorporation of
235 metadata beyond the date of isolation; and typically include a small number of isolates,
236 we additionally examined the regionality of larger clades, usually defined by serotype or
237 genotype (“Manual Lineages”, ML; see Brief Methods and Extended Methods in the SI
238 Appendix for details).

239 The ratio of the inter-lineage to intra-lineage map distances is expected to be
240 greater than unity for regionally defined GLs or MLs, and near or below unity for those
241 lineages that are not regionally defined (Fig. S8). For most viruses analyzed, niches do
242 not appear to be regionally defined, with a few notable exceptions (Fig. S8). In
243 particular, YFV is known to split into three regional lineages (East/Central Africa, West
244 Africa, and South America) although the underlying mechanisms for this separation,
245 especially between the African lineages, are not well understood (10, 11). Similarly,
246 Chikungunya virus (CHIKV) displays regionality although in this case the separation
247 seems to be incomplete (32). WNV lineage 1 can be found globally whereas all other
248 lineages are regional (33). However, evidence of the local co-existence of multiple WNV
249 subtypes (34) indicates that additional WNV niches not linked to regionality might exist.
250 HDV displays weak regionality that might be determined by its helper virus, HBV, on
251 which HDV depends for reproduction. The interplay between HDV and HBV genotypes
252 is not yet well understood (35). Ebola outbreaks show a clear regional structure, which
253 is due to *de novo* spill-over events for each outbreak as well as successful containment
254 measures (30). Some, but not all, GLs for DENV, EVA and EVB may be regionally
255 defined (Fig. S8). Thus while common, regionality does not appear to explain the
256 existence of most apparent niches, although this does not imply absence of spatial
257 separation of localized outbreaks.

258 Similar to regionality, seasonality could potentially support niche formation.
259 Although the temporal resolution of our analysis was limited by the amount of metadata
260 available and the precision with which dates of isolation are specified, we found no
261 evidence that seasonality plays a role in lineage maintenance within viral species. We
262 observed no bi-annual or longer global periodicity of any GLs, but rather a continuous
263 distribution of lineages through time (Figs. S2-7) although shorter temporal patterns are
264 likely for respiratory viruses (36).

265 GLs could represent localized outbreaks (phases of enhanced virus spread)
266 whereby a virus infects only a minute fraction of the global susceptible population at any
267 given time. Under these conditions, even lineages which do not form distinct
268 immunological niches and do not admit near-simultaneous infection, can coexist within
269 short distances of one another. Infection or vaccination leading to life-long immunity as

270 observed, for example, in the case of MMV or MRV (14), can support the emergence of
271 localized outbreaks. In these cases, naïve hosts are born and are not vaccinated, so
272 that a local community of susceptible hosts emerges. Given sufficient evolutionary
273 distance, lineages can become so diverse antigenically that they form different
274 serotypes, which induce weak to no cross-immunity against each other and thus admit
275 near-simultaneous infection. This pattern has been reported for some picornaviruses
276 (12). In the case of zoonotic viruses, distinct lineages can originate when the same virus
277 species is introduced from different animal reservoirs, which could support ongoing
278 diversification and lineage turnover not observed in the human population. This is how
279 some Orthohepevirus A (OHVA) GLs (37) and possibly some TBEV and WNV GLs (33,
280 38) could originate. However, even in this case, the maintenance of multiple niches with
281 low turnover within human populations requires spatiotemporal or immunological
282 separation. Regardless of the specific mechanisms underlying the apparent coexistence
283 of non-competing GLs, we sought to explore lineage-defining mutational signatures and
284 to establish whether significant differences existed between the distributions of
285 mutations within and between lineages.

286

287 **Selective pressures acting on human RNA viruses**

288 Selective processes are often categorized as diversifying, positive, or purifying, in
289 contrast to neutral evolution via genetic drift (39-41). We sought to probe the selective
290 pressures involved in human pathogenic virus evolution by estimating the ratio of non-
291 synonymous to synonymous substitution rates (dN/dS), a gauge of protein-level
292 selection(42, 43). Given that different genes are subject to distinct selective constraints
293 and pressures, the dN/dS value was estimated separately for each viral protein-coding
294 gene (44). Seeking to identify defining features of lineage emergence and maintenance,
295 we would ideally estimate dN/dS across deep and shallow portions of each phylogeny
296 separately. However, because most GLs antedated modern sequencing technologies
297 and therefore few samples located near the root were available, this approach was not
298 feasible. To partially compensate for this lack of data, we compared dN/dS ratios for
299 whole trees, which include deep branches connecting GLs, with those computed over
300 each GL and ML (which are typically larger) individually (see Brief Methods and

301 Extended Methods in the SI Appendix for details). The dN/dS estimates for whole trees
302 ranged between 0.02 and 0.5 for most virus protein-coding genes, which is indicative of
303 strong to moderate purifying selection, in line with previous results (45) (Fig. S9). The
304 few virus genes with elevated dN/dS ratios encode proteins that are either presented on
305 the virion surface, such as HRSV G and M-2 (~3.5x above the species mean dN/dS), or
306 HMPV SH and G (~3 and 5x above the species mean, respectively) (Figs. S9, S10), or
307 are involved in interactions with the host immune system, for example, MMV V protein
308 (46) (~4x above the species mean) (Fig. S10). These proteins are likely to experience
309 positive selection, as described, for example, for HMPV G, where sites under positive
310 selection were identified in the putative ectodomain (47). Elevated dN/dS values were
311 also observed for some very short proteins, for example, the 6k peptide of DENV (Fig.
312 S11). However, such observations are sensitive to statistical artifacts and should be
313 interpreted with caution. For OHVA ORF3, the dN/dS estimate was ~4x above the
314 species mean (0.3, Fig. S13), suggesting that this gene, which encodes an ion channel,
315 plays a role in host adaptation following zoonosis (48).

316 Next, we computed dN/dS for each GL and ML individually (Figs S10-13 and
317 Figs. S14-17, respectively). Despite considerable differences in size, generally, the
318 results for GLs and MLs were comparable. For 12 of the 27 viruses studied (members
319 of the order *Mononegavirales*, HMPV, HRSV, HRV3, MMV and MRV; some flaviviruses
320 ZIKV, YFV, TBEV, YFV; HDV; MERS; and CHIKV) the dN/dS estimates for individual
321 proteins as well as the mean for the whole tree differed little relative to the respective
322 estimates for individual lineages (Figs S10-17), with no indication of how selective
323 pressures might have varied over time for any genes. In contrast, the GLs of
324 enteroviruses (EVA-D) show elevated dN/dS , mainly among capsid proteins (Fig. S16).
325 Although frequent recombination among enteroviruses necessitates interpreting these
326 results with caution (49), this finding, coupled with the observation that mutations in
327 enterovirus capsid protein genes appear to be the primary lineage-defining features
328 (see below), suggests a substantial change in the selective pressure acting on the
329 capsid proteins between the periods of lineage emergence and subsequent
330 maintenance. Notably, OHVA lineages show similarly elevated dN/dS for DUF3729 (up
331 to 0.4) and ORF3 dN/dS (up to 0.3, which is also elevated relative to the species mean

332 as discussed above) (Fig. S17). Both these genes are likely to be involved in host
333 adaptation following zoonosis (37, 48). Further, a two to five fold increase in mean
334 dN/dS was detected for DENV, WNV and HCV GLs across most genes relative to the
335 complete phylogeny (Fig. S15). The interpretation of genome-wide elevation of dN/dS in
336 GLs is more challenging and depends on whether the GL is newly emergent, possibly
337 reflecting a period of rapid host adaptation and intense positive selection (45, 50). Given
338 the distant dates predicted for the LCAs for these GLs and lack of lineage turnover,
339 reduced selective pressure moving from stronger purifying selection towards neutral
340 drift appears more likely. Overall, dN/dS analysis revealed little about potentially
341 differing selective pressures acting within and between GLs despite the apparent
342 differences in substitution rates critical to the definition of the GLs themselves (as
343 discussed above).

344

345 **Intra- and inter-lineage mutational signatures**

346 Gene scale dN/dS analysis is often unable to uncover positive selection acting on
347 specific sites or neighborhoods, which can occur in widely different backgrounds, from
348 neutral drift to strong purifying selection (51). Identification of individual positively
349 selected mutations can provide additional insight into differences between the
350 evolutionary contexts of GL emergence and subsequent maintenance. Multiple, parallel
351 non-synonymous mutations comprise the most obvious indication of site-wise positive
352 selection. With the prominent exception of SARS-CoV-2, for which we have previously
353 identified up to 100 sites with recurrent amino acid replacements that are likely subject
354 to positive selection (52), too few recurrent amino acid substitutions were detected for
355 comparable analysis in the remaining viruses analyzed here despite being the species
356 with the largest number of genome sequences available.

357 Given the infeasibility of the direct, site-specific approach, we performed a
358 genomic neighborhood analysis to compare inter- and intra-lineage mutational
359 signatures. First, amino acid sites were labelled according to three categories of amino
360 acid substitutions (Fig. 4A; see Brief Methods and Extended Methods in the SI
361 Appendix for details): 1) Multiple, deep (MD) substitutions which are “lineage defining”,
362 being conserved in at least 90% of the samples within at least two GLs, but represented

363 by different amino acid residues in each of these GLs. For example, consider the third
364 amino acid of the CHIKV ORF gp1, 97% of the sequences in GL 1 contain a serine in
365 that site, whereas 96% of the sequences in GL2 contain a proline in that site. 2)
366 Multiple, shallow (MS) substitutions occurring on multiple, independent occasions
367 across GLs. 3) All shallow (AS) substitutions occurring at least once within a GL,
368 representing all “recent” events. We then computed site densities for each of these
369 three categories over a sliding window of 101 amino acid sites, respecting protein
370 boundaries.

371 We then examined the correlation between the site densities in these categories
372 of amino acid substitutions across the genome (Fig. 4B and Figs. S18-24). In most
373 cases, there was a strong, positive correlation between all three categories of amino
374 acid substitutions, indicating that most genomic regions are subject to similar selection
375 pressures during inter- and intra-lineage evolution, with several notable exceptions
376 (Fig.4C). For enteroviruses, we observed an elevated MD site density within capsid
377 proteins (VP1-4, Fig. S18-20), suggesting that capsid mutations are primarily lineage-
378 defining, but become less frequent once an epidemiological niche is established and
379 occupied. This trend is consistent with the historical classification of enterovirus
380 lineages by serotype, which is determined by the antigenic properties of the capsid
381 proteins (53). As mentioned above, frequent intra- and inter-species recombination
382 among all 4 types of enteroviruses requires caution when interpreting these results (49).
383 This trend was similarly observed for the capsid proteins of the picornavirus
384 Parechovirus A (PeVA) (VP0, 1C and 1D, Fig. S23).

385 Elevated MD and MS substitution densities were observed for HRSV glycoprotein (G),
386 potentially suggesting multiple residues evolving under positive selection throughout the
387 entire course of evolution (including both lineage emergence and maintenance) of this
388 immunologically exposed protein(54). Both MD and MS substitution densities are also
389 increased in DENV NS2A and CHIKV nsp3. DENV NS2A is involved in virus replication
390 and assembly and shows viroporin-like properties(55, 56). A detailed functional
391 understanding of CHIKV nsp3 is lacking although this protein is known to be part of the
392 replication complex and is also involved in modulating the host cell’s antiviral response
393 (57). In line with the observation of elevated dN/dS in for OHVA DUF3729 in GLs
394 compared to the whole population, MS substitution densities are elevated in this gene
395 (Fig. S22), suggesting that this poorly characterized protein contains multiple positively
396 selected residues. These residues might have played a role in relatively recent host
397 adaptation, but were not necessarily involved in the emergence of multiple lineages.

398 The high MD substitution density observed for large human delta antigen (LHDAG)
399 might result from statistical fluctuations given the short length (20 aa) of this peptide and
400 should be interpreted with caution. As observed for the *dN/dS* analysis, we found few
401 mutational signatures, which would shed light on different selection pressures acting
402 within and between GLs. These observations seem to suggest that, although the tempo
403 is variable, the mode of molecular evolution is broadly conserved from the deep to the
404 shallow portions of each phylogeny, thus, spanning considerable evolutionary distances

405 .

406

407 **Effective population size of human pathogenic RNA viruses**

408 Another tool to indirectly assess the selective pressures shaping a phylogeny is to
409 estimate the effective population size (Ne), which defines the time scale of population
410 turnover across generations and thus can reveal major evolutionary events including
411 population bottlenecks (58). Assuming an evolutionary model, such as Wright-Fisher
412 (59) or Moran (60), one can estimate the number of individuals per generation (that is,
413 Ne) required for the observed rate of turnover in an idealized population. In what
414 follows, we refer to “selection” as the sum of evolutionary pressures that promote
415 lineage turnover. Although the background could vary from strong purifying selection to
416 neutral drift, the occurrence of lineage turnover implicitly assumes some degree of
417 positive selection in most scenarios. In the context of lineage turnover, under strong
418 selection, Ne is small, whereas lack of competition leads to larger Ne values over time
419 (17). Ne can be inferred from the coalescence rate (Cr) estimated for any genealogical
420 tree (17, 61, 62): $Ne * t \sim 1/Cr$ where t is the viral generation time (the time in days a
421 virus needs to complete a transmission cycle from human to human). This expression
422 enables a measurement of diversity and strength of selection among phylogenies
423 represented by a single GL (e.g. H3N2, SARS-CoV-2) as well. Further, the census
424 population size N (individuals present at each generation) can be estimated as $N = D * t$
425 where D is number of yearly cases estimated. The N/Ne ratio may be used to quantify
426 lineage turnover, where $N/Ne \gg 1$ indicates population bottlenecks, and $N/Ne \sim 1$
427 suggests stable population diversity (17). As tree topology, and hence Ne estimates,
428 depend on selection strength and sampling effort (17, 58), we directly assessed the
429 effect of sampling by randomly drawing up to either 10 or 100 samples per year, with
430 three replicates each, for H3N2 and EVA as representative viruses with fast and slow

431 turnover respectively. We then used these reduced ensembles of isolates for
432 genealogical tree construction (see Brief Methods and Extended Methods in the SI
433 Appendix for details, mutation rates and time of LCA shown in Fig. S25). We
434 constructed two additional ensembles for each virus composed of the same number of
435 isolates selected above, this time maximizing the sequence diversity (as measured by
436 the hamming distance between alignment rows, see Brief Methods and Extended
437 Methods in the SI Appendix for details). As a result, we obtained six trees evenly
438 sampled over time (3x, e10 and e100) as well as two maximally diverse subtrees of the
439 same size (d10 and d100) for both H3N2 and EVA.

440 We calculated the coalescence rates for all complete trees and for the H3N2 and
441 EVA subtrees using the PACT package (<http://www.trevorbedford.com/pact> (17)) and
442 estimated N_e (Fig. 5A). The N_e estimation was not performed for some zoonotic viruses
443 including TBEV and WNV, for which the generation time could not be reliably estimated.
444 N/N_e ratios were calculated based on the best estimates of N_e for complete trees and
445 those obtained after even and diverse sampling (H3N2 and EVA), (Fig. 5A and 5B). The
446 estimated N_e values span more than two orders of magnitude with H3N2e10 and EVD
447 representing the extremes (Fig. 5A, N_e of around 400 and 270,000 respectively).
448 Sampling was found to have a major effect on the estimates. The N_e estimates for EVA
449 d100, d10, e100, and the whole tree were similar, whereas EVA e10 was about an
450 order of magnitude lower. It should be noted that EVA e100 contained most sequences
451 present in the whole tree. This trend was even more pronounced for H3N2 where the
452 N_e estimates for d100, d10, and the whole tree were similar, whereas those for e10 and
453 e100 were several orders of magnitude lower. It is first important to note that the
454 estimates were not sensitive to the number of sequences present in the phylogeny as
455 illustrated by the equivalency of d10 and the whole phylogeny for both viruses,
456 indicating that the differences observed between e10 and e100 and the whole
457 phylogeny are not merely methodological artifacts. However, the estimate is sensitive to
458 sampling and, as could be expected, this sensitivity is more pronounced for viruses with
459 fast lineage turnover. While perhaps unsurprising, this finding implies that N_e has been,
460 and likely continues to be in this work, underestimated due to data limitations for most
461 viruses and H3N2 in particular.

462 To illustrate the potential equivalency of reduced sampling and increased
463 selection on Ne estimation, we simulated an ensemble of genealogical trees under a
464 simple phenomenological model. Trees were iteratively constructed through the addition
465 of clades representing local sequencing efforts. Increased sequencing efforts were
466 modelled by changing the number of sequences in each clade from 2 to 6. Increased
467 selection strength was modelled by changing the placement of these clades on the tree,
468 relative to the root, from the prior iteration. A root distance threshold was set to be the
469 0th, 25th, 50th, 75th, or 95th percentile of the root distance distribution for all leaves at
470 the prior iteration with higher thresholds corresponding to new isolates being placed
471 farther from the tree root and representing increased selection (Fig. 5C, Fig. S26A-C).
472 Although selection and under-sampling result in qualitatively different tree topologies
473 (Fig. 5D), their effects cannot be disentangled from Ne analysis alone. Furthermore,
474 sensitivity to under-sampling is more pronounced under high selection than under low
475 selection (Fig. 5D, Fig. S26D). These effects must be considered when evaluating the
476 expectation that genetic diversity (and hence Ne) plateaus earlier in a growing census
477 population N when selection is strong (17). This challenge is reflected in the damped
478 increase of Ne from H3N2 e10 to e100 when compared to the increase from EVA e10 to
479 e100 (~4- and 8-fold, respectively; Fig. 5A).

480 Keeping these sensitivities in mind, we proceeded to examine the N/Ne ratios.
481 High N/Ne ratios can be an indicator of population bottlenecks. The highest N/Ne ratio
482 was observed for H3N2e10 (e100 was similar); in contrast, the estimate for the whole
483 phylogeny was about 200-fold lower (Fig. 5D), within the range of the majority of the
484 other viruses. Thus, sampling efforts can substantially affect the interpretation of the
485 N/Ne estimation, moving H3N2 from an outlier associated with extreme bottlenecks to
486 typical behavior. As discussed above, it has been well established that H3N2 is subject
487 to pronounced population bottlenecks as a result of alternating periods of stasis and
488 rapid host adaptation (16-18). However, the results presented here emphasize that on
489 shorter timescales the transmission dynamics of local outbreaks play a larger role in
490 determining the extent of the diversity of the H3N2 population (63) as was the case for
491 the majority of viruses studied in this work,. BCoV1 also demonstrated a high N/Ne
492 ratio, within the range of H3N2 e10 and e100 (Fig. 5B). Although this observation could

493 simply result from insufficient sampling, given the high incidence of this virus (Fig.
494 S27D), it might point to pronounced population bottlenecks during the evolution of the
495 BCoV1 population (although not of comparable magnitude to those for H3N2; see
496 below). In contrast, other viruses seem to experience less severe bottlenecks and
497 maintain greater genetic diversity (e.g. MRV and enteroviruses A, C, D). The low N/Ne
498 values for MERS, ZIKV and CHIKV likely result from an underestimation of N due to
499 large animal reservoirs that might impact estimates of N for H3N2 as well.

500 Whereas insufficient sampling can lead to an underestimation of both N and Ne ,
501 the complete unavailability of genomes from premodern periods can, perhaps
502 counterintuitively, lead to an overestimation of Ne . As discussed above, GLs are
503 separated by periods (branches of the tree) with apparently different substitution rates.
504 These branches are often deep within the tree topology and sparsely populated with
505 leaves (if at all), making the assignment of a global model for substitution rates
506 statistically dubious. This can result in inaccurate deep branch lengths for genealogical
507 trees and substantially change the predicted date for the LCA. This date, as well as the
508 predicted dates of other deep nodes, is used to estimate the effective population size.
509 Given these limitations, we sought to establish a lower bound for the effective
510 population size, which still preserves all GLs, through the construction of truncated
511 global genealogical trees or “grafted trees”. The LCA of each grafted tree is set to the
512 LCA of the oldest GL and the remaining GLs are connected to this (multifurcated) root
513 through branches preserving the LCA of each respective GL (see Fig. S27A and Brief
514 Methods or Extended Methods in the SI Appendix for details). We proceeded to
515 estimate Ne for each grafted tree as well as for each GL separately (Fig. S27B). By
516 construction, Ne estimates for grafted trees are generally significantly smaller than
517 those for complete trees and larger than those for individual GLs. Notably, the Ne
518 estimate for H3N2 (which is represented by a single GL) is the second highest value
519 observed (after RVA) among the viruses studied when this lower bound is considered.
520 This counterintuitive finding emphasizes another facet of the sensitivity of Ne estimation
521 to data availability.

522 These sensitivities are evidently greater within individual GLs, which represent
523 only a subset of the viral diversity for each species. These limitations notwithstanding, in

524 an effort to characterize lineage turnover within individual GLs, we analyzed skyline
525 plots representing the time to the most recent common ancestor (TMRCA) of all clades
526 present at a given time point and diversity within the population over time (as measured
527 by the average time for any two isolates to coalesce, that is, to find their most recent
528 common ancestor) for individual GLs and the complete population (Fig. S28). The
529 average population diversity can be displayed as the mean diversity per year (Fig.
530 S28A). Populations with high turnover, such as H3N2, show a low average diversity per
531 year, whereas those with low turnover are characterized by high diversity. In general,
532 the skyline plots and mean diversity values for complete phylogenies correspond well to
533 N_e and N/N_e estimations, supporting slow lineage turnover for most of the viruses
534 analyzed. For example, H3N2 displays ~4x and ~8x lower mean diversity/year
535 compared to BCoV1 and ZIKV respectively. This observation suggests BCoV1, despite
536 having high N_e and N/N_e values, has a slower population turnover compared to H3N2.
537 Of note, evidence of high intra-GL turnover was obtained for few GLs (as demonstrated
538 by a mean diversity in the range of H3N2 or BCoV1). The two principal examples are
539 HRSV GL2 and Norwalk GL3 (Fig. S28C, D). The majority of the GLs show mean
540 diversity within the range of viral populations with low turnover.

541

542 **Discussion**

543 Here we present a comprehensive phylodynamic analysis of monopartite human
544 pathogenic RNA viruses (and H3N2 hemagglutinin) in an effort to establish global
545 trends in viral evolution in human populations. Despite data limitations, the viruses
546 studied in this work span a wide variety of viral life history characteristics. This lends
547 considerable generality to the study, while making it outside the scope of this work to
548 investigate many features specific to individual lifestyles (for example, intra-host
549 diversity, symptom characteristics, or acute vs. chronic infection (2)). Given this
550 diversity, the commonalities we observe among the virus phylogenies constructed are
551 notable. Consistent with the conclusions of previous efforts (45, 64), we observed
552 moderate to strong purifying selection among all viruses.

553 Nearly all virus populations are characterized by low rates of lineage turnover,
554 and most consist of multiple, coexisting GLs, monophyletic groups of sequences

555 separated by periods with apparently different substitution rates. Despite these differing
556 substitution rates, dN/dS and genomic neighborhood analysis revealed little about how
557 selective pressures might have differed between the early period of GL formation and
558 the subsequent period defined by persistent coexistence. This lack of resolution seems
559 to suggest that, although the tempo is variable, the mode of molecular evolution is
560 broadly conserved from the deep to the shallow portions of each phylogeny, spanning
561 considerable evolutionary distances. The distribution of lineage-defining mutations
562 across the virus genome is similar to that of shallow, repeated mutations for almost all
563 viruses, indicating that positive selection affects sites in the same neighborhoods during
564 both periods (Fig. 4). The lineage-defining role of enterovirus capsid proteins was the
565 principle exception observed, in line with the traditional serotype classification (12).
566 Other virus proteins with different intra- and inter-lineage mutational signatures, which
567 might provide insight into ongoing host and/or vector adaptive evolution, are OHVA
568 DUF3729, DENV NS2A, and CHIKV NSP3. In the case of CHIKV E1-A226V, NSP3 has
569 been demonstrated to play an important role in the adaptation to the vector *Aedes*
570 *albopictus* (65). In general, the low GL turnover and broadly stable mutational
571 signatures appear to be indicative of weak if any competition among GLs, suggesting
572 that each GL occupies an independent epidemiological niche (Fig. 5).

573 Such niches could be maintained in a variety of ways, the most obvious
574 possibility being regionality and/or seasonality. Although these factors can explain the
575 persistence of some GLs identified in this work, the majority do not show regional
576 localization, and none display biannual (or more coarse-grained) temporal trends (the
577 limit of time resolution we can reliably detect). At sufficiently large evolutionary
578 distances, niches can be defined by immunological differences, which can overcome
579 immune cross-protection allowing the same host to be infected by multiple
580 subpopulations largely independent of prior infections as seems to be the case for
581 picornaviruses and HRSV (54). These effects are also insufficient to account for the
582 stability of most GLs. We suggest that, in many if not most cases, niches are maintained
583 through a series of localized outbreaks such that only a small fraction of the global
584 susceptible population is infected at any given time. Under this scenario, even lineages
585 that do not overcome immune cross-protection can coexist within short distances of one

586 another. Furthermore, extensive environmental transfer or fragmented animal reservoir
587 populations could play a role. Virions that can persist for extended periods of time
588 outside of the (identified) host or vector might maintain the genetic diversity of a lineage
589 during time periods when no active infections from that lineage occur.

590 As a result of globalization, disparate communities are becoming increasingly
591 connected, which might lead to increased interaction between previously separated
592 lineages, enhancing between-lineage competition within the viral population. This effect
593 has been demonstrated already for DENV in Thailand where multiple lineages typically
594 coexist throughout the country with a well-defined pattern of dissemination. However,
595 within densely populated areas of Bangkok, genomic analysis pointed to increased
596 competition and lineage turnover (66).

597

598 **Conclusions**

599 Phylodynamic analysis revealed multiple co-circulating lineages (GLs) for the
600 majority of human pathogenic RNA viruses separated by periods of apparently different
601 substitution rates within the phylogeny. *dN/dS* and genomic neighborhood analysis
602 yielded surprisingly little evidence of different selection pressures acting within and
603 between GLs, suggesting that whereas the tempo is variable, the mode of molecular
604 evolution is broadly conserved. This slow lineage turnover suggests each GL occupies
605 an independent epidemiological niche, with little inter-GL competition. No pronounced
606 patterns of regional or temporal separation of the GLs were detected, suggesting that
607 the stability of the GLs primarily stems from limited outbreaks within small communities
608 so that only a small fraction of the global susceptible population is infected at any time.
609 These results raise the, perhaps pressing, question: how will increased host-host
610 contact resulting from globalization affect viral evolution? Could new or renewed
611 competition emerge among lineages of endemic viruses to drive diversification,
612 evolution of increased pathogenicity, or even virus speciation? With these questions in
613 mind, we emphasize that, in addition to zoonotic events, the ongoing surveillance of
614 familiar, endemic viruses deserves global attention in effort to mitigate or prevent future
615 pandemics.

616

617

618 **Author contributions**

619 PM, NDR, and GF collected data; PM, NDR, YIW, GF, FZ, and EVK analyzed data; PM,
620 NDR, and EVK wrote the manuscript that was edited and approved by all authors.

621

622 **Acknowledgements**

623 The authors thank Koonin group members for helpful discussions. NDR, YIW, PM, and
624 EVK are supported by the Intramural Research Program of the National Institutes of
625 Health (National Library of Medicine).

626

627 **Brief Methods**

628 **Multiple Sequence Alignments of RNA Virus Genomes**

629 Genomes were retrieved for all viruses except influenza A virus H3N2 and SARS-CoV-2
630 from NCBI virus (24). Members of related viral families were used to construct an
631 outgroup when possible. Influenza A virus H3N2 (flu H3N2) segment HA was retrieved
632 from the NCBI flu database (67). The SARS-CoV-2 tree and alignment analyzed in this
633 work was subsampled from a larger alignment consisting of all high quality genomes
634 that were available as of January 8, 2021 in the GISAID database(25), as previously
635 described (52). Subsampling was conducted to maximize the sequence diversity.
636 Acknowledgments for the GISAID deposited sequences used in this study are displayed
637 in Supplementary Data, Table S3. Subalignments were considered for H3N2 and EVA,
638 principally for the purpose of effective population size analysis. In all cases sequences
639 were harmonized to DNA (e.g. U was transformed to T to amend software compatibility)
640 and aligned with MAFFT(26), using default settings. Sequences were clustered
641 according to 100% identity with no coverage threshold using CD-HIT (68), and
642 otherwise default settings for MERS and H3N2.

643 The longest sequence from each cluster was selected as a representative. Exterior
644 ambiguous characters were removed, and sequences with more than 10 remaining
645 ambiguous characters (“N”) were discarded. Outliers based on hamming distance to the
646 nearest neighbor and consensus were identified and removed from the set. Sites
647 corresponding to protein-coding ORFs were then mapped to the alignments and
648 noncoding regions were discarded. Common gaps corresponding to multiples of three
649 nucleotides were maintained as “true” insertions or deletions and mapped into frame if
650 necessary. Unique alignment rows were identified. Samples related to laboratory
651 experiments, vaccine-related sequences and patents were pruned based on an
652 automated keyword search

653 Dates and locations of isolation are available for many isolates reported as calendar
654 dates and city or country/administrative region of origin. These dates are referenced as
655 calendar dates in the main text and date indices (number of days before/after January
656 1, 1950) in the supplement. For the regional analysis, the latitude and longitude of each
657 city of origin or a representative city for each country/administrative region of origin was
658 identified from simplemaps (<https://simplemaps.com/data/world-cities>) (69).

659 With the exception of SARS-CoV-2 and H3N2, tree topology was optimized using IQ-
660 TREE (27) with the evolutionary model fixed to GTR+F+G4 and the minimum branch
661 length decreased from the default 10e-6 to 10e-7 (options: -m GTR+F+G4 -st DNA -
662 blmin 0.0000001). For SARS-CoV-2, the tree was drawn from the global topology
663 previously described (52). The global H3N2 tree was approximated using FastTree(70)
664 specifying GTR; a 4 category gamma distribution; no support values; and using a
665 previously-constructed maximum diversity subtree as a constraint (compiled at double
666 precision, options: -nt -gtr -gamma -cat 4 -nosupport -constraints). Trees were rooted
667 according to the position of an outgroup when possible and by date or midpoint
668 otherwise.

669 Viral lineages were both manually selected based on available metadata and
670 algorithmically into correlated-clades we call “genealogical lineages” or GLs. GLs are
671 defined as monophyletic clades with a strong correlation between the sequencing date
672 and the distance to the tree root. Trees were used to construct date-constrained,
673 genealogical trees using least-square dating (with software LSD2) (31). We considered
674 the Shannon entropy of the clade distribution calculated over sliding windows based on
675 the known or estimated date of isolation OR distance to the tree root as an explicit
676 measure of lineage turnover.

677 Fitch Traceback (71) was used to estimate ancestral states. Three classes of amino
678 acid sites were identified on the basis of the nonsynonymous mutations within each site.
679 1) Multiple, deep (MD) substitutions are “lineage defining”. 2) Multiple, shallow sites. 3)
680 All shallow sites. We computed the site density of each class over a sliding window to
681 assess signatures of positive selection. Selection pressures were also assessed
682 through *dN/dS* analysis using PAML(44).

683 The effective population size N_e and the ratio of the census population size N over N_e
684 was estimated as previously described (17) <http://www.trevorbedford.com/pact>. Viral
685 diversity (average time of any pair of leaves at a given timepoint to find their LCA) and
686 average time to most recent common ancestor (TMRCA) over time were calculated with
687 the PACT package as well. In order to demonstrate the potential equivalency between
688 the impacts of selection strength and sampling density on effective population size, we
689 additionally simulated an ensemble of trees.

690 List of abbreviations

691 **AS:** All, shallow

692 **BCoV1:** Betacoronavirus 1

693 **CHIKV:** Chikungunya virus

694 **DENV:** Dengue virus

695 **dN/dS:** ratio of non-synonymous to synonymous substitution rates

696 **DUF:** Domain of unknown function

697 **Ebola:** Zaire ebolavirus

698 **EVA:** Enterovirus A

699 **EVAd:** Enterovirus A 'diverse'

700 **EV Ae:** Enterovirus A 'even'

701 **EVB:** Enterovirus B

702 **EVC:** Enterovirus C

703 **EV Ce:** Enterovirus C 'every' sample

704 **EV Cr:** Enterovirus C 'reduced' samples

705 **EVD:** Enterovirus D

706 **GL:** Genealogical lineage

707 **H3N2d:** H3N2 'divers'

708 **H3N2e:** H3N2 'even'

709 **HBV:** Hepatitis B virus

710 **HCV:** Hepatitis C virus

711 **HC Ve:** Hepatitis C virus 'every' sample

712 **HC Vr:** Hepatitis C virus 'reduced' samples

713 **HDV:** Hepatitis D virus

714 **HMPV:** Human metapneumovirus

715 **HRSV:** Human respiratory syncytial virus

716 **HRV3:** Human respirovirus 3

717 **H3N2:** Influenza A Virus H3N2

718 **LCA:** Last common ancestor

719 **LHD_{Ag}**: Large human delta antigen
720 **LSD**: least-square distance
721 **MD**: Multiple, deep
722 **MERS**: Middle East respiratory syndrome-related coronavirus
723 **ML**: Manual lineage
724 **MMV**: Measles morbillivirus
725 **MRCA**: Most recent common ancestor
726 **MRV**: Mumps rubulavirus
727 **MS**: Multiple, shallow
728 **N**: Census population size
729 **Ne**: Effective population size
730 **Norwalk**: Norwalk virus
731 **NS**: Non-structural protein
732 **NSP**: Non-structural protein
733 **OHVA**: Orthohepevirus A
734 **PeVA**: Parechovirus A
735 **RVA**: Rhinovirus A
736 **SARS-CoV-2**: Severe acute respiratory syndrome-related coronavirus 2
737 **SV**: Sapporo virus
738 **TMRCA**: Time to most recent common ancestor
739 **YFV**: Yellow fever virus
740 **ZIKV**: Zika virus
741

742 **Declarations**

743 **Ethics approval and consent to participate**

744 Not applicable.

745

746 **Consent for publication**

747 Not applicable.

748

749 **Data Availability**

750 The datasets generated and/or analyzed during the current study are available as
751 supplementary data at Zenodo, <https://doi.org/10.5281/zenodo.5711959>, as well as
752 through FTP, https://ftp.ncbi.nih.gov/pub/wolf/_suppl/virNiches/. Original virus
753 sequences are publicly available for all viruses except SARS-CoV-2 at NCBI virus (24).
754 SARS-CoV-2 sequences are available at GISAID (25).

755

756 **Competing interests**

757 The authors declare that they have no competing interests.

758

759 **Funding**

760 NDR, YIW PM, and EVK are supported by the Intramural Research Program of the
761 National Institutes of Health (National Library of Medicine).

762

763 **Authors' contributions**

764 PM, NDR, and GF collected data; PM, NDR, YIW, GF, FZ, and EVK analyzed data; PM,
765 NDR, and EVK wrote the manuscript that was edited and approved by all authors.

766

767 **Acknowledgements**

768 The authors thank Koonin group members for helpful discussions.

769

770

771 References

772

773 1. Suttle CA (2007) Marine viruses--major players in the global ecosystem. *Nat Rev Microbiol* 5(10):801-812.

774 2. Chisholm PJ, Busch JW, & Crowder DW (2019) Effects of life history and ecology on virus

775 evolutionary potential. *Virus Res* 265:1-9.

776 3. Johnson PT, de Roode JC, & Fenton A (2015) Why infectious disease research needs community

777 ecology. *Science* 349(6252):1259504.

778 4. Yan L, Neher RA, & Shraiman BI (2019) Phylodynamic theory of persistence, extinction and

779 speciation of rapidly adapting pathogens. *Elife* 8.

780 5. Marchi J, Lässig M, Mora T, & Walczak AM (2019) Multi-Lineage Evolution in Viral Populations

781 Driven by Host Immune Systems. *Pathogens* 8(3).

782 6. WHO WHO (2021) Coronavirus (COVID-19) Dashboard.

783 7. Harvey WT, *et al.* (2021) SARS-CoV-2 variants, spike mutations and immune escape. *Nat Rev*

784 *Microbiol* 19(7):409-424.

785 8. Rochman N, Wolf Y, & Koonin E (2021) Evolution of human respiratory virus epidemics [version

786 2; peer review: 2 approved]. *F1000Research* 10(447).

787 9. Simmonds P, Aiewsakun P, & Katzourakis A (2019) Prisoners of war - host adaptation and its

788 constraints on virus evolution. *Nat Rev Microbiol* 17(5):321-328.

789 10. Bryant JE, Holmes EC, & Barrett AD (2007) Out of Africa: a molecular perspective on the

790 introduction of yellow fever virus into the Americas. *PLoS Pathog* 3(5):e75.

791 11. Li Y & Yang Z (2017) Adaptive Diversification Between Yellow Fever Virus West African and South

792 American Lineages: A Genome-Wide Study. *Am J Trop Med Hyg* 96(3):727-734.

793 12. Brouwer L, Moreni G, Wolthers KC, & Pajkrt D (2021) World-Wide Prevalence and Genotype

794 Distribution of Enteroviruses. *Viruses* 13(3).

795 13. Geoghegan JL & Holmes EC (2018) Evolutionary Virology at 40. *Genetics* 210(4):1151-1162.

796 14. Grenfell BT, *et al.* (2004) Unifying the epidemiological and evolutionary dynamics of pathogens.

797 *Science* 303(5656):327-332.

798 15. Kim H, Webster RG, & Webby RJ (2018) Influenza Virus: Dealing with a Drifting and Shifting

799 Pathogen. *Viral Immunol* 31(2):174-183.

800 16. Wolf YI, Viboud C, Holmes EC, Koonin EV, & Lipman DJ (2006) Long intervals of stasis punctuated

801 by bursts of positive selection in the seasonal evolution of influenza A virus. *Biol Direct* 1:34.

802 17. Bedford T, Cobey S, & Pascual M (2011) Strength and tempo of selection revealed in viral gene

803 genealogies. *BMC Evol Biol* 11:220.

804 18. Koelle K, Cobey S, Grenfell B, & Pascual M (2006) Epochal evolution shapes the phylodynamics

805 of interpandemic influenza A (H3N2) in humans. *Science* 314(5807):1898-1903.

806 19. Rota PA, *et al.* (2016) Measles. *Nat Rev Dis Primers* 2:16049.

807 20. Hamblin SR, White PA, & Tanaka MM (2014) Viral niche construction alters hosts and

808 ecosystems at multiple scales. *Trends Ecol Evol* 29(11):594-599.

809 21. Volz EM, Koelle K, & Bedford T (2013) Viral phylodynamics. *PLoS Comput Biol* 9(3):e1002947.

810 22. Houldcroft CJ, Beale MA, & Breuer J (2017) Clinical and biological insights from viral genome

811 sequencing. *Nat Rev Microbiol* 15(3):183-192.

812 23. Liu L (2014) Fields Virology, 6th Edition. *Clinical Infectious Diseases* 59(4):613-613.

813 24. Hatcher EL, *et al.* (2017) Virus Variation Resource - improved response to emergent viral

814 outbreaks. *Nucleic Acids Res* 45(D1):D482-d490.

815

816 25. Shu Y & McCauley J (2017) GISAID: Global initiative on sharing all influenza data—from vision to
817 reality. *Eurosurveillance* 22(13):30494.

818 26. Katoh K, Misawa K, Kuma Ki, & Miyata T (2002) MAFFT: a novel method for rapid multiple
819 sequence alignment based on fast Fourier transform. *Nucleic acids research* 30(14):3059-3066.

820 27. Nguyen L-T, Schmidt HA, Von Haeseler A, & Minh BQ (2015) IQ-TREE: a fast and effective
821 stochastic algorithm for estimating maximum-likelihood phylogenies. *Molecular biology and*
822 *evolution* 32(1):268-274.

823 28. Scholle SO, Ypma RJ, Lloyd AL, & Koelle K (2013) Viral substitution rate variation can arise from
824 the interplay between within-host and epidemiological dynamics. *Am Nat* 182(4):494-513.

825 29. Organisation WH (2021) Ebola virus disease fact-sheets. (who).

826 30. Jacob ST, *et al.* (2020) Ebola virus disease. *Nat Rev Dis Primers* 6(1):13.

827 31. To T-H, Jung M, Lycett S, & Gascuel O (2016) Fast dating using least-squares criteria and
828 algorithms. *Systematic biology* 65(1):82-97.

829 32. Schneider AB, *et al.* (2019) Updated Phylogeny of Chikungunya Virus Suggests Lineage-Specific
830 RNA Architecture. *Viruses* 11(9).

831 33. Chancey C, Grinev A, Volkova E, & Rios M (2015) The global ecology and epidemiology of West
832 Nile virus. *Biomed Res Int* 2015:376230.

833 34. Di Giallonardo F, *et al.* (2016) Fluid Spatial Dynamics of West Nile Virus in the United States:
834 Rapid Spread in a Permissive Host Environment. *J Virol* 90(2):862-872.

835 35. Wang W, *et al.* (2021) Assembly and infection efficacy of hepatitis B virus surface protein
836 exchanges in eight hepatitis D virus genotype isolates. *J Hepatol.*

837 36. Moriyama M, Hugentobler WJ, & Iwasaki A (2020) Seasonality of Respiratory Viral Infections.
838 *Annu Rev Virol* 7(1):83-101.

839 37. Lin S & Zhang YJ (2021) Advances in Hepatitis E Virus Biology and Pathogenesis. *Viruses* 13(2).

840 38. Kubinski M, *et al.* (2020) Tick-Borne Encephalitis Virus: A Quest for Better Vaccines against a
841 Virus on the Rise. *Vaccines (Basel)* 8(3).

842 39. Dolan PT, Whitfield ZJ, & Andino R (2018) Mechanisms and Concepts in RNA Virus Population
843 Dynamics and Evolution. *Annu Rev Virol* 5(1):69-92.

844 40. Lynch M, *et al.* (2016) Genetic drift, selection and the evolution of the mutation rate. *Nat Rev
845 Genet* 17(11):704-714.

846 41. Kimura M (1991) The neutral theory of molecular evolution: a review of recent evidence. *Jpn J
847 Genet* 66(4):367-386.

848 42. Hurst LD (2002) The Ka/Ks ratio: diagnosing the form of sequence evolution. *Trends Genet*
849 18(9):486.

850 43. Hejase HA, Dukler N, & Siepel A (2020) From Summary Statistics to Gene Trees: Methods for
851 Inferring Positive Selection. *Trends Genet* 36(4):243-258.

852 44. Yang Z (2007) PAML 4: phylogenetic analysis by maximum likelihood. *Molecular biology and
853 evolution* 24(8):1586-1591.

854 45. Lin JJ, Bhattacharjee MJ, Yu CP, Tseng YY, & Li WH (2019) Many human RNA viruses show
855 extraordinarily stringent selective constraints on protein evolution. *Proc Natl Acad Sci U S A*
856 116(38):19009-19018.

857 46. Takeuchi K, Kadota SI, Takeda M, Miyajima N, & Nagata K (2003) Measles virus V protein blocks
858 interferon (IFN)-alpha/beta but not IFN-gamma signaling by inhibiting STAT1 and STAT2
859 phosphorylation. *FEBS Lett* 545(2-3):177-182.

860 47. Papenburg J, *et al.* (2013) Genetic diversity and molecular evolution of the major human
861 metapneumovirus surface glycoproteins over a decade. *J Clin Virol* 58(3):541-547.

862 48. Primadharsini PP, Nagashima S, & Okamoto H (2021) Mechanism of Cross-Species Transmission,
863 Adaptive Evolution and Pathogenesis of Hepatitis E Virus. *Viruses* 13(5).

864 49. Kyriakopoulou Z, Pliaka V, Amoutzias GD, & Markoulatos P (2015) Recombination among human
865 non-polio enteroviruses: implications for epidemiology and evolution. *Virus Genes* 50(2):177-
866 188.

867 50. Holmes EC (2003) Patterns of intra- and interhost nonsynonymous variation reveal strong
868 purifying selection in dengue virus. *J Virol* 77(20):11296-11298.

869 51. Kryazhimskiy S & Plotkin JB (2008) The population genetics of dN/dS. *PLoS Genet*
870 4(12):e1000304.

871 52. Rochman ND, *et al.* (2021) Ongoing global and regional adaptive evolution of SARS-CoV-2. *Proc
872 Natl Acad Sci U S A* 118(29).

873 53. Oberste MS, Maher K, Kilpatrick DR, & Pallansch MA (1999) Molecular evolution of the human
874 enteroviruses: correlation of serotype with VP1 sequence and application to picornavirus
875 classification. *J Virol* 73(3):1941-1948.

876 54. Wertz GW & Moudy RM (2004) Antigenic and genetic variation in human respiratory syncytial
877 virus. *Pediatr Infect Dis J* 23(1 Suppl):S19-24.

878 55. Neufeldt CJ, Cortese M, Acosta EG, & Bartenschlager R (2018) Rewiring cellular networks by
879 members of the Flaviviridae family. *Nat Rev Microbiol* 16(3):125-142.

880 56. Shrivastava G, *et al.* (2017) NS2A comprises a putative viroporin of Dengue virus 2. *Virulence*
881 8(7):1450-1456.

882 57. Fros JJ & Pijlman GP (2016) Alphavirus Infection: Host Cell Shut-Off and Inhibition of Antiviral
883 Responses. *Viruses* 8(6).

884 58. Wang J, Santiago E, & Caballero A (2016) Prediction and estimation of effective population size.
885 *Heredity (Edinb)* 117(4):193-206.

886 59. Ishida Y & Rosales A (2020) The origins of the stochastic theory of population genetics: The
887 Wright-Fisher model. *Stud Hist Philos Biol Biomed Sci* 79:101226.

888 60. Moran PAP (1958) Random processes in genetics. *Mathematical Proceedings of the Cambridge
889 Philosophical Society* 54(1):60-71.

890 61. Strimmer K & Pybus OG (2001) Exploring the demographic history of DNA sequences using the
891 generalized skyline plot. *Mol Biol Evol* 18(12):2298-2305.

892 62. Pybus OG, Rambaut A, & Harvey PH (2000) An integrated framework for the inference of viral
893 population history from reconstructed genealogies. *Genetics* 155(3):1429-1437.

894 63. McCrone JT & Lauring AS (2018) Genetic bottlenecks in intraspecies virus transmission. *Curr
895 Opin Virol* 28:20-25.

896 64. Wertheim JO & Kosakovsky Pond SL (2011) Purifying selection can obscure the ancient age of
897 viral lineages. *Mol Biol Evol* 28(12):3355-3365.

898 65. Tsetsarkin KA, *et al.* (2014) Multi-peaked adaptive landscape for chikungunya virus evolution
899 predicts continued fitness optimization in Aedes albopictus mosquitoes. *Nat Commun* 5:4084.

900 66. Salje H, *et al.* (2017) Dengue diversity across spatial and temporal scales: Local structure and the
901 effect of host population size. *Science* 355(6331):1302-1306.

902 67. Bao Y, *et al.* (2008) The influenza virus resource at the National Center for Biotechnology
903 Information. *J Virol* 82(2):596-601.

904 68. Li W & Godzik A (2006) Cd-hit: a fast program for clustering and comparing large sets of protein
905 or nucleotide sequences. *Bioinformatics* 22(13):1658-1659.

906 69. simplemaps (2021) World Cities Database.

907 70. Price MN, Dehal PS, & Arkin AP (2010) FastTree 2—approximately maximum-likelihood trees for
908 large alignments. *PLoS one* 5(3):e9490.

909 71. Fitch WM (1971) Toward defining the course of evolution: minimum change for a specific tree
910 topology. *Systematic Biology* 20(4):406-416.

911 72. Wolf YI, *et al.* (2018) Origins and Evolution of the Global RNA Virome. *mBio* 9(6).

913 **Figure legends**

914

915 **Figure 1. Phylogenies of human pathogenic RNA viruses**

916 Schematic depicting the origins and phylogenetic tree topologies of 27 human
917 pathogenic RNA viruses.

918 **A.** Placement of each virus in the global phylogeny of RNA viruses (realm Riboviria).

919 The tree topology is from (72). Viral groups containing human pathogenic viruses
920 are named in black if containing viruses analyzed in this work and gray otherwise.
921 The numbers of viral species, for which at least 200 nearly complete genome
922 sequences were available, at least 50 of these isolated from humans, are shown in
923 colored circles (green: monopartite viruses; blue: segmented viruses).

924 **B.** Speciation of viral families or orders.

925 **C.** Diversification within species. Trees for species are scaled to the same distance
926 from the root to the most distal leaf and are grafted on the tree scaffold with arbitrary
927 branch lengths for speciation but respecting topology.

928

929 **Figure 2. Stable Coexistence of Lineages among Human Pathogenic RNA Viruses**

930 **A.** EVD tree colored to represent the location of the three genealogical lineages (GL).

931 **B.** Distance to the tree root vs. date of isolation for EVD. Distance is scaled by the
932 maximum for any sequence within a correlated-clade and the x axis is bounded by
933 the minimum/maximum date of isolation for any such sequence.

934 **C.** The fraction of isolates within each correlated-clade (and excluding isolates that did
935 not belong to any correlated-clade) computed over a sliding window containing the
936 nearest 5% of all isolates indexed by sequencing date (top) and root distance
937 (bottom, where date* represents the date of isolation corresponding to each
938 sequence in an alternative phylogeny where the date of isolation for each sequence
939 exactly corresponds to the distance to the root for that sequence).

940 **D.** The mean Shannon entropy for the correlated-clade distribution respecting the
941 sequencing date (y-axis, $\langle S_t^j \rangle_j$) and root distance (x-axis, $\langle S_d^j \rangle_j$) respectively. Dashed
942 line displays $\langle S_t^j \rangle_j = \langle S_d^j \rangle_j$.

943

944 **Figure 3. Genealogical lineages of human pathogenic RNA viruses throughout**
945 **time**

946 **A.** Mutation rates (substitutions per site per year) for all main and GL phylogenetic trees
947 used to construct genealogical trees (top). Time to Last Common Ancestor (LCA) in
948 years from 2021 for all main and GL populations used to construct genealogical
949 trees (bottom).

950 **B.** Number of GLs per virus species circulating at the same time, based on the
951 genealogical trees for each GL. For unannotated samples within a GL, the sampling
952 date was estimated based on the date of the MRCA and root distance.

953

954 **Figure 4. Mutational Signatures in human pathogenic RNA viruses vary little with**
955 **tree depth**

956 **A.** Illustration of three amino acid site classes considered. 1) Multiple, deep (MD, red).
957 2) Multiple, shallow (MS, yellow). 3) All, shallow (AS, blue). Dashed circle represents
958 deep, singular mutations which are excluded from this analysis.

959 **B.** Pearson correlation coefficient between site densities for all pairs of site classes
960 across the genome computed over a moving average of 101 amino acids respecting
961 mature peptide boundaries. Rows are sorted by the first column subtracted from the
962 third column.

963 **C.** Log ratio of the mean site density across the specified peptide relative to the whole
964 genome for select peptides. Bars are bounded by the 25th and 75th percentiles of
965 simulated data drawn from the binomial distribution with $n=\text{total number of sites}$
966 across the genome trials of probability $p=\text{length of peptide} / \text{length of genome}$.
967 RVA|P* represents the union of peptides P2-C, P-3A, and protease-3C.

968

969 **Figure 5. Estimation of effective population sizes for human pathogenic RNA**
970 **viruses**

971 **A.** N_e estimated for genealogical trees. Bars represent varying generation time t for
972 each virus ranging between 0.5 and 5 times the value corresponding to the filled
973 circle. For H3N2 and EVA, N_e estimates for evenly sampled trees (up to 10 or 100

974 samples per year, e10 and e100, respectively) and diverse sampled trees (d10 and
975 d100) are also displayed.

976 **B.** N/Ne ratios, where N is the census population. Bars represent varying N between
977 0.5 and 5 times the value corresponding to the filled circle. N and t estimates are
978 shown in Supplementary Data, Table S10. As in (C), N/Ne estimates are shown for
979 evenly and diverse sampled trees for EVA and H3N2. Colour code as in (C).

980 **C.** Ne (with t fixed to 1 for all trees) for simulated trees varying selection strength and
981 sampling density (Ne represented by circle area).

982 **D.** Example simulated trees resulting from simulations of varying selection strength and
983 sampling density.

Fig. 1

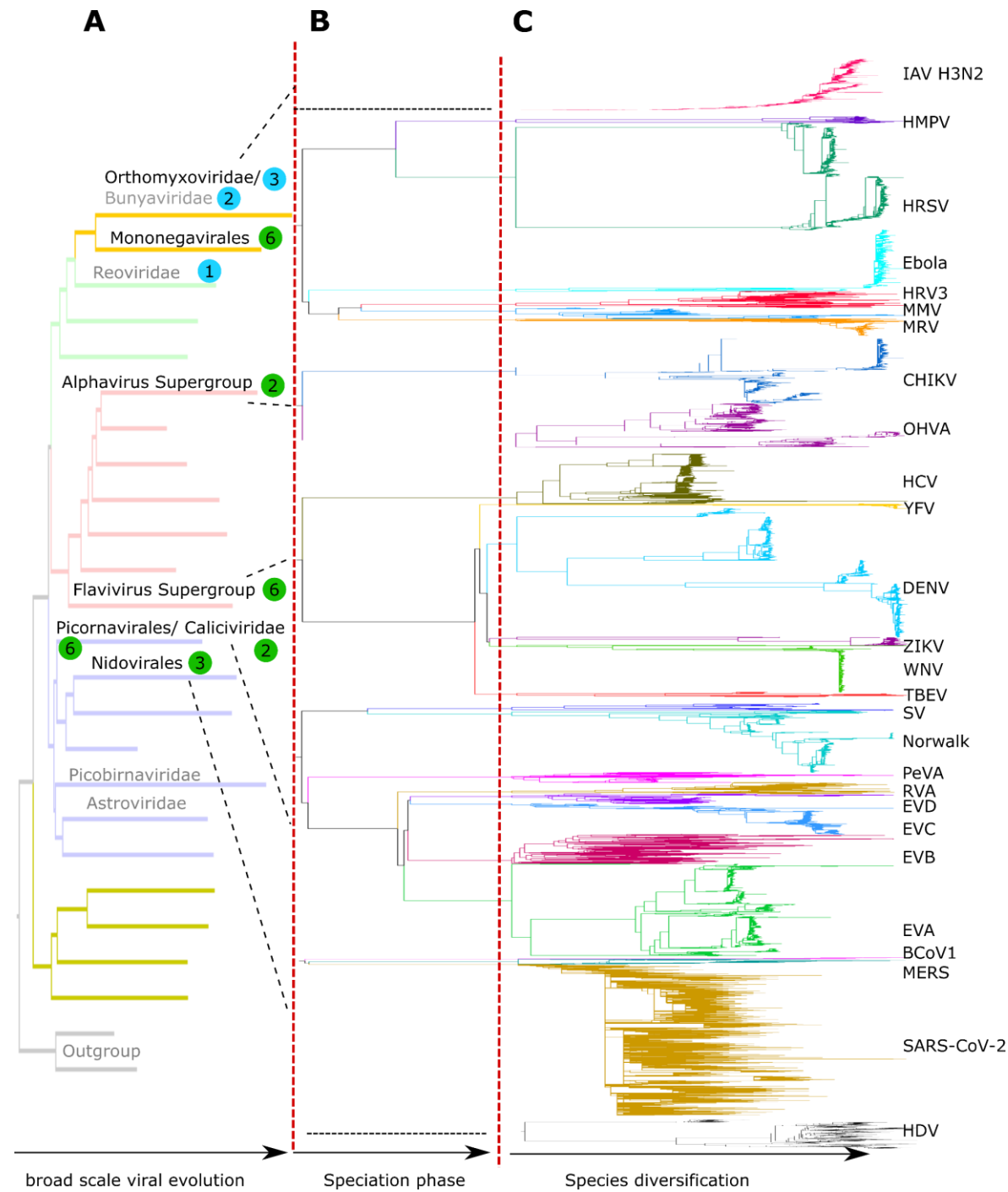


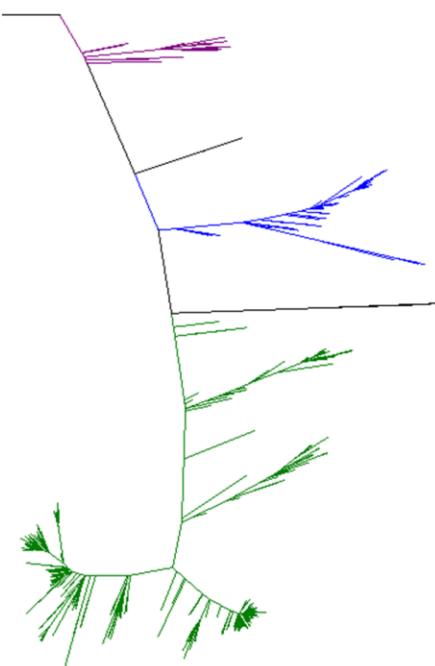
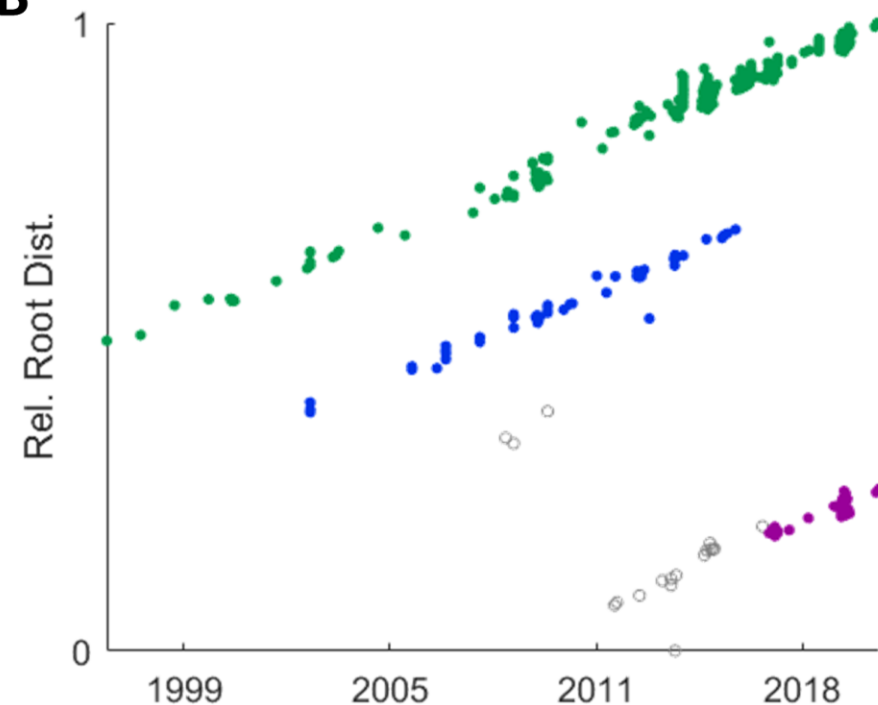
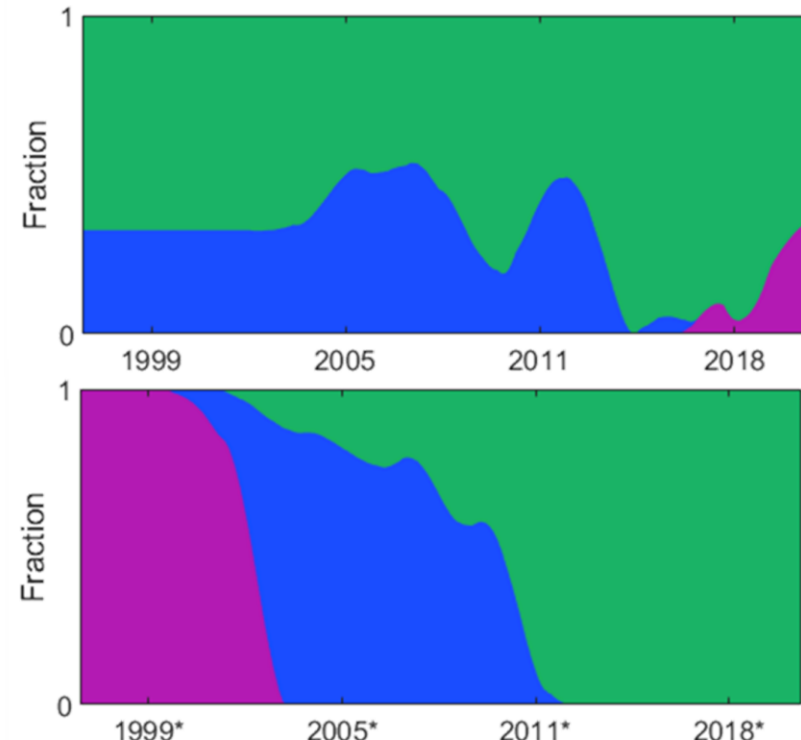
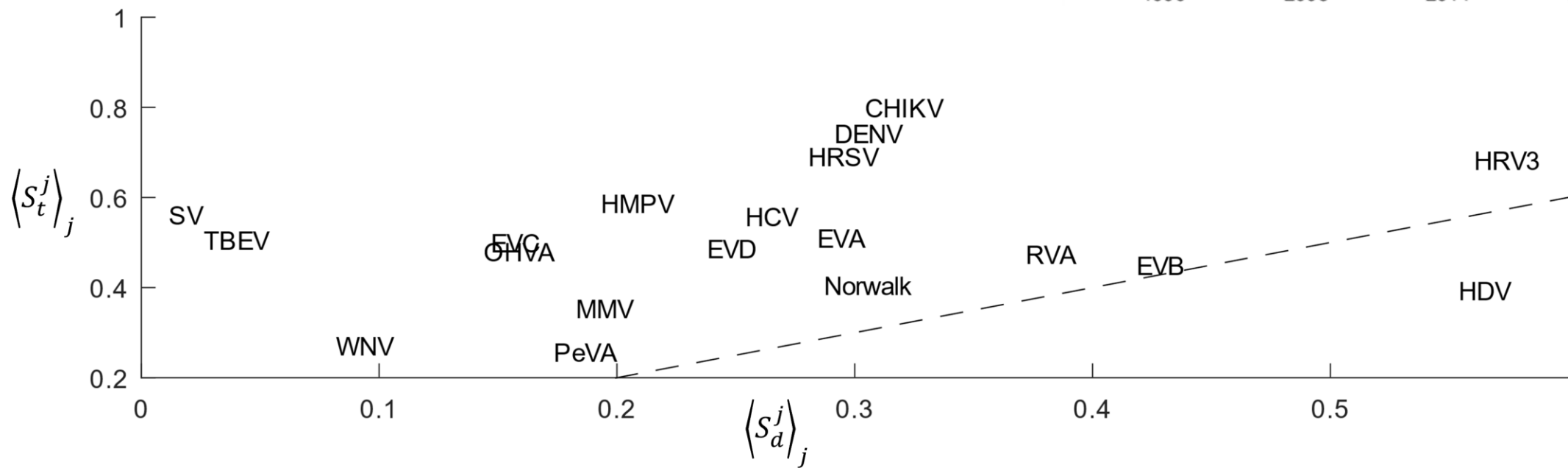
Fig. 2 A**B****C****D**

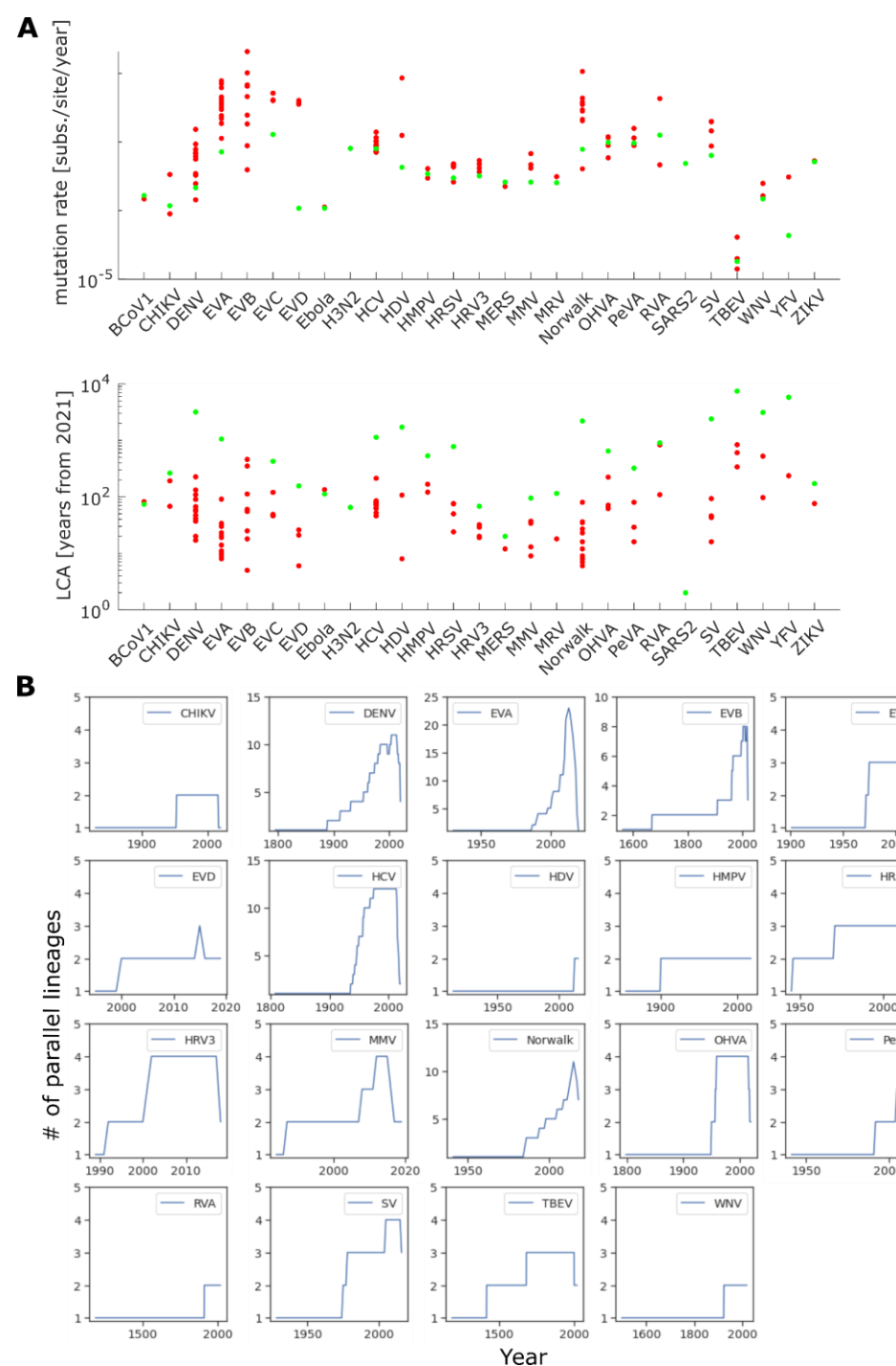
Fig. 3

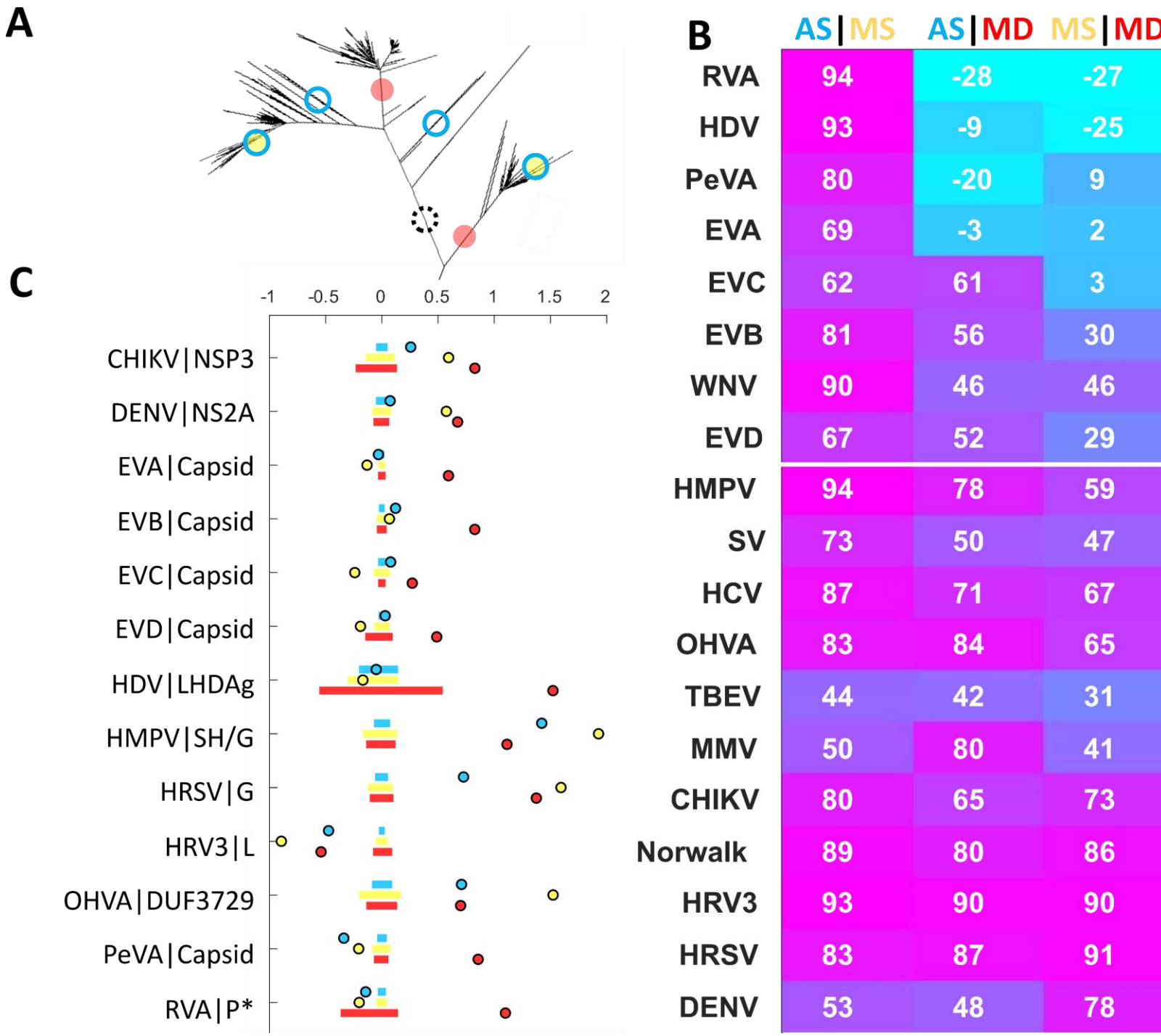
Fig. 4

Fig. 5